

Magnetic cluster expansion model for bcc-fcc transitions in Fe and Fe-Cr alloys

M. Yu. Lavrentiev, D. Nguyen-Manh, and S. L. Dudarev

EURATOM/CCFE Fusion Association, Abingdon, Oxfordshire OX14 3DB, United Kingdom

(Received 24 March 2010; published 6 May 2010)

An *ab initio*-based magnetic-cluster-expansion treatment developed for body- and face-centered cubic phases of iron and iron-chromium alloys is applied to modeling the α - γ and γ - δ phase transitions in these materials. The Curie, Néel, and the structural phase-transition temperatures predicted by the model are in good agreement with experimental observations, indicating that it is the thermal excitation of magnetic *and* phonon degrees of freedom that stabilizes the fcc γ phase. The model also describes the occurrence of the γ loop in the phase diagram of Fe-Cr alloys for a realistic interval of temperatures and Cr concentrations.

DOI: [10.1103/PhysRevB.81.184202](https://doi.org/10.1103/PhysRevB.81.184202)

PACS number(s): 64.75.Op, 61.43.-j, 61.50.Ks, 75.50.Bb

I. INTRODUCTION

The occurrence of body-centered cubic (bcc) to face-centered cubic (fcc) α - γ and fcc-bcc γ - δ structural phase transitions in pure iron, and the so-called γ loop in the phase diagram of Fe-Cr alloys, are the key physical phenomena determining the manufacturing and processing routes, the low- and high-temperature mechanical properties, and the type of defect structures formed under irradiation in steels developed for nuclear fission and fusion applications.¹ Surprisingly little is known about the microscopic origin of these transitions, or about the factors determining the stability region for the fcc phase (the γ loop), treated as a function of temperature and Cr concentration. Hasegawa and Pettifor² explained the transitions between bcc, fcc, and hcp phases of pure iron by comparing the magnetic free energies evaluated using the single-site spin-fluctuation theory of band magnetism. However, because their model neglected the short-range magnetic order, the authors of Ref. 2 were unable to predict correctly the fact that the observed Curie temperature for bcc α iron is lower than the temperature of the α to γ transition. Other authors^{3,4} modeled the structural transitions using semi-empirical interatomic potentials, making no distinction between the magnetic and vibrational degrees of freedom. A recent *ab initio*-based study of bcc iron below $T_{\alpha-\gamma}$ (Ref. 5) provided estimates for the magnetic, electronic, and vibrational contributions to the Helmholtz free energy. Yet no attempt has succeeded so far in developing a self-consistent first-principles-based treatment for the α - γ and γ - δ phase transitions in Fe-Cr alloys, which are the main constituents of many industrial steels.

In this paper we show that an *ab initio*-parameterized magnetic-cluster-expansion (MCE) model, combining the cluster-expansion treatment of configurational alloy disorder with a multidimensional symmetry-breaking Landau expansion for transverse and longitudinal thermal magnetic fluctuations and including, where necessary, the phonon free energy derived from experimental data, is able to predict the characteristic temperatures for magnetic (Curie and Néel) *and* structural phase transitions for a broad range of Fe-Cr alloy compositions.

Predicting the occurrence of a phase transition requires evaluating the free energies of competing phases and computing their difference. For the case of the α - γ bcc-fcc tran-

sition in iron, the difference between the free energies of the two phases in the region where fcc Fe is stable is very small (of the order of several meV). To prove this, we estimate the fcc-bcc free-energy difference using a three-point parabolic fit. Noting that the free energies of the two phases coincide at the α - γ and γ - δ transition temperatures ($T_{\alpha-\gamma}=1185$ K and $T_{\gamma-\delta}=1667$ K, respectively⁶), and estimating the difference between the energies of the two phases at $T=0$ K from our density functional theory (DFT) calculations as $\Delta E_0 \sim 100$ meV/atom, we find that the fcc-bcc free-energy difference in the middle of the region of stability for the γ phase equals approximately $-\Delta E_0(T_{\gamma-\delta}-T_{\alpha-\gamma})^2/4T_{\alpha-\gamma}T_{\gamma-\delta} \approx -3$ meV/atom. Thermodynamic analysis of experimental data predicts even smaller values, which are on the order of -1 meV/atom.^{6,7}

Theoretical studies of fcc γ -Fe are mostly limited to *ab initio* investigations of the rich variety of its electronic and magnetic structures. Apart from the low-spin and high-spin ferromagnetic states,⁸ fcc γ -Fe exhibits a number of antiferromagnetically ordered phases. Herper *et al.*⁹ identified an antiferromagnetic double-layer structure as the lowest-energy collinear magnetic phase. The noncollinear magnetic structures have the form of complex antiferromagnetic spin spirals^{10,11} found experimentally in γ -Fe precipitates embedded in a Cu matrix.¹² Neutron-diffraction data¹³ show that antiferromagnetic order in γ -Fe vanishes above 67 K. Fcc γ -Cr does not exist at ambient conditions but *ab initio* methods provide means for evaluating the energy difference between its fcc and bcc phases.¹⁴⁻¹⁷ The lowest-energy state of fcc Cr is antiferromagnetic and the predicted fcc-bcc energy difference lies in a range between 370 (Ref. 17) and 435 (Ref. 16) meV/atom.

This complexity of electronic and magnetic structures increases further for the fcc Fe-Cr alloys, where *ab initio* data are very scarce. Mirzoev *et al.*¹⁷ found that the enthalpy of mixing is negative for the fcc phase in the entire alloy composition range. The available models for the γ loop in the phase diagram of Fe-Cr alloys do not go beyond relatively simple thermodynamic estimates.¹⁷⁻¹⁹

II. MAGNETIC-CLUSTER-EXPANSION HAMILTONIAN

The MCE model²⁰ is a *magnetic symmetry-breaking* extension and generalization of the cluster expansion (CE)

approach.^{21,22} While CE only treats the configurational disorder in an alloy, and hence does not predict the occurrence of the γ phase in iron, an MCE Hamiltonian includes the magnetic vector variables and describes the magnetic degrees of freedom for the atoms forming the alloy. It allows the ground-state magnetic configuration to self-consistently adjust, via magnetic symmetry breaking, to an atomic configuration.

The MCE model is fundamentally different to recent regular non-symmetry-breaking parametrizations for the magnetic energy, the so-called spin-cluster expansion²³ and a rotationally invariant representation of the magnetic energy in terms of bilinear products of direction vectors of the moments.²⁴ The energy of an alloy configuration in the MCE model depends on the discrete atomic CE occupational variables σ_i ($\sigma_i=+1$ for Fe and $\sigma_i=-1$ for Cr) and on the classical magnetic moments \mathbf{M}_i of the constituent atoms. These magnetic moments have variable direction *and* magnitude, enabling MCE to describe the alloy in terms of its atomic configuration and its corresponding magnetic state. The treatment is also different from the Ising model,²⁵ where moments have fixed magnitude, but is somewhat similar to the 1983 model by Hasegawa and Pettifor² where the magnetic moments also have variable magnitude and direction (up or down).

It is easy to see that in order to describe the energies of atomic configurations in a magnetic alloy, it is essential to treat magnetic moments as parameters that have variable direction and magnitude. *Ab initio* calculations show that in Fe-Cr alloys the magnitude of magnetic moments on Cr sites varies between $0.2\mu_B$ and $1.9\mu_B$, whereas the range of variation associated with Fe sites is even broader (the “length” of the magnetic moments varies from $0.2\mu_B$ to $2.3\mu_B$), depending on the alloy composition and short-range atomic order. Estimates based on the Stoner model^{26,27} show that the variation in magnitude of magnetic moments on the scale noted above gives rise to the variation in magnetic energy on the scale ~ 200 meV/atom.

An MCE Hamiltonian is a sum of conventional “scalar” CE terms, the self-energy symmetry-breaking magnetic terms defining the magnitude of atomic magnetic moments, and the intersite Heisenberg-type magnetic interaction terms. The self-energy part of the Hamiltonian is given by a sum of atomic-configuration-dependent Landau expansion terms quadratic and quartic in \mathbf{M}_i . In general, the Hamiltonian includes atomic clusters of any size. In the treatment developed here we retain only the two-atom clusters in both magnetic and nonmagnetic expansions

$$\begin{aligned}
 E(\{\sigma_i\}, \{\mathbf{M}_i\}) = & N I^{(0)} + I^{(1)} \sum_i \sigma_i + \sum_{ij} J_{ij}^{(2)} \sigma_i \sigma_j \\
 & + \sum_i \left(A^{(0)} + A^{(1)} \sigma_i + \sigma_i \sum_j A_{ij}^{(2)} \sigma_j \right) \mathbf{M}_i^2 \\
 & + \sum_i \left(B^{(0)} + B^{(1)} \sigma_i + \sigma_i \sum_j B_{ij}^{(2)} \sigma_j \right) \mathbf{M}_i^4 \\
 & + \sum_{ij} \left(J_{ij}^{(0)} + J_{ij}^{(1)} (\sigma_i + \sigma_j) + J_{ij}^{(2)} \sigma_i \sigma_j \right) \mathbf{M}_i \cdot \mathbf{M}_j.
 \end{aligned}
 \tag{1}$$

In this equation $I^{(i)}$ are the nonmagnetic CE coefficients, $A^{(i)}$ and $B^{(i)}$ are the configuration-dependent Landau expansion coefficients for the magnetic self-energy terms, and $J^{(i)}$ are the magnetic interaction coefficients. Summation over i and j involves atoms occupying the nearest-neighbor coordination shells. The functional form of Eq. (1) guarantees that the magnetic self-energy terms, and hence the directions and magnitudes of magnetic moments \mathbf{M}_i predicted by the model, depend on the local environment of each atom in the alloy.

The MCE parameters for pure fcc iron were fitted using *ab initio* data on energies and magnetic moments for nonmagnetic, ferromagnetic, and several collinear antiferromagnetic structures. *Ab initio* data were generated using Vienna *Ab Initio* Simulation Package (VASP) in the generalized gradient approximation with projected augmented wave pseudopotentials.²⁸ The calculations were performed for spin-polarized configurations using the generalized gradient approximations and verified by comparing the energies found using the exchange-correlation functionals by Perdew and Wang, and by Perdew, Burke, and Ernzerhof. The set of MCE parameters for fcc iron includes three magnetic interaction coefficients $J_{1NN}^{fcc}(\text{Fe-Fe}) = J_{1NN}^{(0)} + 2J_{1NN}^{(1)} + J_{1NN}^{(2)} = -0.650$ meV, $J_{2NN}^{fcc}(\text{Fe-Fe}) = 0.267$ meV, and $J_{3NN}^{fcc}(\text{Fe-Fe}) = 0.233$ meV, as well as the self-energy terms $A^{fcc}(\text{Fe}) = A^{(0)} + A^{(1)} + 12A_{1NN}^{(2)} + 6A_{2NN}^{(2)} = -65.022$ meV, and $B^{fcc}(\text{Fe}) = 6.513$ meV. The first nearest-neighbor magnetic interaction coefficient favors ferromagnetic ordering whereas the second and the third nearest-neighbor coefficients favor antiferromagnetic ordering of moments. The set of MCE parameters for pure bcc iron²⁰ involves only the first and the second nearest-neighbor coefficients, both favoring ferromagnetic ordering, namely: $J_{1NN}^{bcc}(\text{Fe-Fe}) = -3.097$ meV and $J_{2NN}^{bcc}(\text{Fe-Fe}) = -2.426$ meV, $A^{bcc}(\text{Fe}) = -148.35$ meV, and $B^{bcc}(\text{Fe}) = 18.876$ meV.

Monte Carlo simulations were performed using bcc and fcc cells containing in excess of 1.6×10^4 lattice sites. At each Monte Carlo step, an attempt is made to vary the magnetic moment of a randomly chosen atom. Both the direction and magnitude of vectors \mathbf{M}_i are treated as variables. For the case of Fe-Cr alloys, random alloy configurations were selected for both bcc and fcc structures to simulate high-temperature configurational disorder effects. The equilibration and statistics accumulation stages involved approximately 4×10^4 Monte Carlo steps per atom. Despite the fact that only the collinear magnetic structures were used for fitting the MCE parameters of expansion in Eq. (1) to *ab initio* data, the predicted lowest-energy magnetic structure of fcc Fe was found to be noncollinear antiferromagnetic. The energy of this configuration is by 0.5 meV/atom lower than the energy of a collinear double-layer structure and by 17 meV/atom lower than the energy of a ferromagnetic configuration. We note that it is difficult to derive the experimentally observed incommensurate spin spiral configuration¹² from a generalized Heisenberg model.¹¹

III. STRUCTURAL PHASE TRANSITIONS IN Fe AND Fe-Cr

The magnetic part of the specific heat for bcc and fcc iron, exhibiting peaks corresponding to magnetic order-disorder

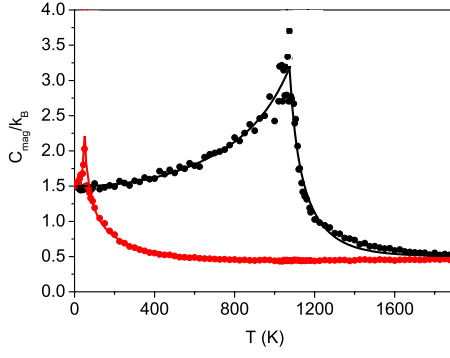


FIG. 1. (Color online) The magnetic part of the specific heat for bcc (black circles) and fcc (red circles) iron. Lines are fits to the calculated data, see text.

phase transitions, is shown in Fig. 1. In the limit of low temperatures, our model predicts that the specific heat equals $3k_B/2$ for both the bcc and fcc phases. For fcc iron, the magnetic specific heat is maximum at $T_N \sim 50$ K. The occurrence of this peak corresponds to vanishing antiferromagnetic long-range order of magnetic moments at T_N . The predicted T_N is close to the observed Néel temperature of fcc iron $T_N = 67$ K.¹³ The predicted Curie temperature of bcc α -Fe also agrees with experimental observations. The magnetic specific heat is maximum at $T_C \approx 1075$ K,²⁰ which is only slightly higher than the observed Curie temperature $T_C = 1043$ K. The calculated specific-heat data were fitted for both systems using the expressions similar to those used by Chen and Sundman⁶ in their comprehensive survey of experimental data, resulting in the following expressions (shown in Fig. 1 as solid lines):

$$\begin{aligned}
 C_{mag}^{bcc}/k_B &= \frac{3}{2} + a_1 \left[\left(\frac{T}{1075} \right)^{\alpha_1} + \frac{1}{3} \left(\frac{T}{1075} \right)^{3\alpha_1} \right. \\
 &\quad \left. + \frac{1}{5} \left(\frac{T}{1075} \right)^{5\alpha_1} \right], \quad T \leq 1075 \text{ K}, \\
 C_{mag}^{bcc}/k_B &= \frac{1}{2} + a_2 \left[\left(\frac{1075}{T} \right)^{\alpha_2} + \frac{1}{3} \left(\frac{1075}{T} \right)^{3\alpha_2} \right. \\
 &\quad \left. + \frac{1}{5} \left(\frac{1075}{T} \right)^{5\alpha_2} \right], \quad T > 1075 \text{ K}, \quad (2) \\
 C_{mag}^{fcc}/k_B &= \frac{3}{2} + b_1 \left[\left(\frac{T}{50} \right)^{\beta_1} + \frac{1}{3} \left(\frac{T}{50} \right)^{3\beta_1} + \frac{1}{5} \left(\frac{T}{50} \right)^{5\beta_1} \right], \\
 &\quad T \leq 50 \text{ K}, \\
 C_{mag}^{fcc}/k_B &= \frac{1}{2} + b_2 \left[\left(\frac{50}{T} \right)^{\beta_2} + \frac{1}{3} \left(\frac{50}{T} \right)^{3\beta_2} + \frac{1}{5} \left(\frac{50}{T} \right)^{5\beta_2} \right] \\
 &\quad + 0.0000712654T - 0.25865 \\
 &\quad + 0.17886 \exp\left(\frac{50 - T}{215.0038} \right), \quad T > 50 \text{ K}, \quad (3)
 \end{aligned}$$

where $a_1 = 1.1$, $a_2 = 1.72353$, $\alpha_1 = 2.22531$, $\alpha_2 = 9.61649$, b_1

$= 0.33149$, $b_2 = 1.11185$, $\beta_1 = 2.1617$, and $\beta_2 = 0.70687$. Chen and Sundman⁶ used for both phases the values of 3 and 7 for the low- and high-temperature exponents, respectively. Comparison shows that our fit gives similar exponents for the bcc Fe (α_1 and α_2). The high-temperature exponent for the γ -Fe (β_2) in our simulations is much smaller than the one used by the authors of Ref. 6. It should be noted that experimental data on the specific heat of fcc Fe are not available and there is no reason to expect that the exponents noted above should be equal for the bcc and fcc phases.

The temperatures of the α - γ and γ - δ transitions correspond to the crossover points for the free energies of the respective phases. The magnetic free energy is given by the difference between the magnetic energy and entropy terms

$$F_{mag}^\gamma - F_{mag}^\alpha = E_{mag}^\gamma - E_{mag}^\alpha - T(S_{mag}^\gamma - S_{mag}^\alpha), \quad (4)$$

where the magnetic-entropy difference is evaluated using the Nernst integrals for the magnetic specific heat. Numerical integration was carried out by performing summation over more than one hundred calculated points in the temperature range 0–1900 K. The results were verified by integrating the fitted curves (2–3). The difference between the values found using the two methods does not exceed 0.3 meV/atom in the temperature range $T \geq 1200$ K.

The phonon contribution to the free energy of bcc α -iron was derived from experimental elastic constants measured for the highest available temperature, 1173 K, at which bcc iron remained mechanically stable.²⁹ From elastic moduli we deduce the three dominant force constants α_1 , β_1 , and α_2 .³⁰ The resulting dynamical matrix is then diagonalized at 4.2×10^7 points in an irreducible wedge of the Brillouin zone. For fcc γ iron we use a force-constants model³¹ derived from experimental data on inelastic neutron scattering at 1428 K and perform diagonalization of the dynamical matrix at 8.4×10^7 points in an irreducible wedge of the Brillouin zone.

The γ - α free-energy difference derived from MCE simulations, and various terms contributing to it, are shown in Fig. 2(a) as functions of temperature. We see that both the magnetic and phonon excitations contribute to the free energies of the α , γ , and δ phases. The magnetic γ - α energy difference decreases monotonically in the entire temperature range. Changes in the slope of the $\Delta E_{mag}(T)$ curve at very low temperatures and near 1000 K are related to the Néel and Curie magnetic phase transitions in fcc and bcc Fe, respectively. The difference between the energies of fcc and bcc phases decreases by more than 100 meV/atom between the Néel and the Curie temperatures. The magnetic entropy term is responsible for the minimum of $\Delta F_{mag}(T)$, and for its upward trend at high temperatures. The temperature dependence of the vibrational free-energy difference at temperatures that are much higher than the Debye temperatures of bcc and fcc Fe (473 and 324 K, respectively^{31,32}) is almost linear. By adding this contribution, we arrive at a function $\Delta F_{tot}(T)$ that takes negative values over a certain temperature range and hence exhibits the occurrence of two structural phase transitions.

Figure 2(b) gives a magnified view of the high-temperature part of the MCE free-energy curve. For comparison, Fig. 2(b) also shows the data derived from the ther-

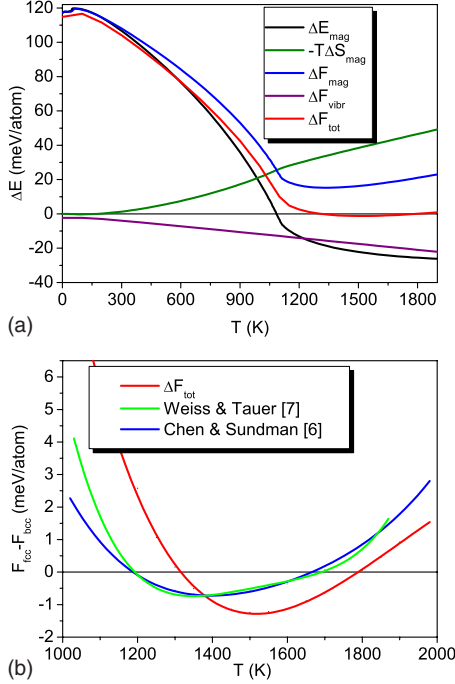


FIG. 2. (Color online) Difference between the free energies of fcc γ -Fe and bcc α -Fe phases $\Delta F_{tot} = F^\gamma - F^\alpha$, and its constituent parts plotted (a) for the entire temperature range investigated in this study and (b) for the α - γ transition region.

modynamic analysis of experimental observations.^{6,7} The phase-transition temperatures predicted by the MCE model are within 10% of experimentally observed values. For example, we find $T_{\alpha\gamma}^{(MCE)} = 1315$ K and $T_{\gamma\delta}^{(MCE)} = 1795$ K, compared to $T_{\alpha\gamma}^{(exp)} = 1185$ K and $T_{\gamma\delta}^{(exp)} = 1667$ K.⁶ The minimum value for the fcc-bcc free-energy difference predicted by the MCE model is close to -1 meV/atom, in agreement with thermodynamics.

Applying MCE to Fe-Cr alloys requires parameterizing the model to include Fe-Cr and Cr-Cr interactions. For fcc Cr *ab initio* calculations predict almost identical energies for the nonmagnetic and magnetic structures, and the difference between the energies of fcc and bcc chromium at $T=0$ K is $E^{fcc}(\text{Cr}) - E^{bcc}(\text{Cr}) = 403$ meV/atom. Since the γ loop only occurs in the interval of low Cr concentration $x_{\text{Cr}} < 11.9$ at. %, we fitted the MCE parameters to *ab initio* data for three structures with $x_{\text{Cr}} = 0.0625$ and $x_{\text{Cr}} = 0.125$, as well as to pure Cr, with predictive rms error for the energies of ~ 12 meV/atom. The magnetic interaction coefficients are given in Table I. The self-energy magnetic terms for pure fcc chromium are $A^{fcc}(\text{Cr}) = A^{(0)} - A^{(1)} + 12A_{1NN}^{(2)} + 6A_{2NN}^{(2)} = 0.828$ meV, $B^{fcc}(\text{Cr}) = 5.226$ meV, $A_{1NN}^{(2)} = 2.884$ meV, $A_{2NN}^{(2)} = 0.365$ meV, $B_{1NN}^{(2)} = -0.123$ meV, and $B_{2NN}^{(2)} = -0.003$ meV. The nonmagnetic-cluster-expansion coefficients for the first and the second nearest neighbors are -3.624 and -3.638 meV, respectively.

For bcc Fe-Cr we use an improved MCE parameters fit, compared to the one reported previously.²⁰ The new fit does not include the high-energy B2 crystal structure since the interference effects in the electronic band structure for this crystal configuration are not well described by a classical

TABLE I. Magnetic interaction parameters for Fe-Cr MCE Hamiltonian (meV).

	Neighbor	$J(\text{Fe-Fe})$	$J(\text{Fe-Cr})$	$J(\text{Cr-Cr})$
Bcc	1NN	-3.097	19.881	5.555
	2NN	-2.426	12.380	6.890
	3NN	0	-0.266	3.432
	4NN	0	-2.322	6.984
	5NN	0	0	7.374
Fcc	1NN	-0.650	1.022	-0.009
	2NN	0.267	-0.956	0.065
	3NN	0.233	0	0

MCE Hamiltonian. The parameters characterizing Fe-Cr magnetic interactions were amended by using DFT data on energies and magnetic moments for 14 Fe-Cr structures, without revising the MCE parameters for pure Fe and Cr. The rms predictive error for the energies of these structures is ~ 11 meV/atom. This can be compared, e.g., with the predictive error of ~ 7 meV/atom achieved for Fe-Cr in the conventional cluster expansion, using a larger database of 74 input structures.²² The improved magnetic interaction parameters set, which predicts the maximum enthalpy of mixing for a random Fe-Cr solution of 68 meV/atom at $T=0$ K, is in agreement with CALPHAD (Ref. 33) and the earlier CE data.³⁴ The numerical values of MCE parameters are given in Table I. The self-energy magnetic terms for pure bcc chromium are $A^{bcc}(\text{Cr}) = -59.898$ meV, $B^{bcc}(\text{Cr}) = 56.694$ meV, $A_{1NN}^{(2)} = -4.652$ meV, $A_{2NN}^{(2)} = 4.601$ meV, $B_{1NN}^{(2)} = 0.201$ meV, and $B_{2NN}^{(2)} = -1.738$ meV. The nonmagnetic-cluster-expansion coefficients for the first and the second nearest neighbors in bcc Fe-Cr are -1.529 and -2.514 meV, respectively.

The temperature range of stability for γ iron is well above the top of the miscibility gap for bcc Fe-Cr. For fcc Fe-Cr there is full miscibility at all temperatures. Assuming the ideal configurational entropy for both phases in the temperature range corresponding to the occurrence of the γ loop, we write the free-energy difference $\Delta F(x) = F^{fcc}(x) - F^{bcc}(x)$ for $\text{Fe}_{1-x}\text{Cr}_x$ alloy as

$$\Delta F(x) = (1-x)\Delta F(\text{Fe}) + x\Delta F(\text{Cr}) + \Delta H_{mix}(x) + \Delta F_{vibr}(x). \quad (5)$$

The dependence of the phonon free energy on the chromium content for bcc Fe-Cr alloys was estimated from the variation in the dominant force constants between pure Fe and $\text{Fe}_{0.7}\text{Cr}_{0.3}$ observed in experiments on inelastic neutron scattering.³⁵ For fcc Fe-Cr, linear regression of experimental data on elastic constants for several Fe-Cr-Ni alloys³⁶ was performed in order to estimate the dependence of elastic constants and force constants on the chromium content.

The difference between the free energies of fcc and bcc phases predicted by the MCE model is shown in Fig. 3. In the limit of small chromium concentration and high temperatures, the combination of negative ΔH_{mix}^{fcc} and positive ΔH_{mix}^{bcc} stabilizes the γ phase. The region where fcc γ -Fe-Cr is more stable than bcc α -Fe-Cr extends to 10.5% Cr, in agreement

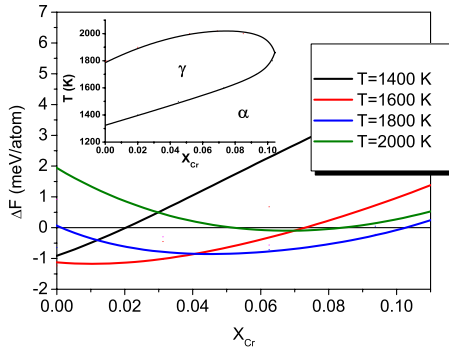


FIG. 3. (Color online) Difference between the free energies of fcc and bcc $\text{Fe}_{1-x}\text{Cr}_x$ alloys plotted as a function of chromium content x_{Cr} . The predicted γ loop is shown in the inset.

with the experimental phase diagram showing that the γ loop extends to 11.9 at. % Cr. For higher Cr concentrations, the large positive $\Delta F(\text{Cr})$ restabilizes the bcc α phase. The shape of the γ loop predicted by MCE is slightly different from the shape observed experimentally, where at small Cr concentrations the lower part of the γ loop shifts down the temperature axis. The exact position of the γ loop is determined by the concentration dependence of $\Delta H_{\text{mix}}(x) = H_{\text{mix}}^{\text{fcc}}(x) - H_{\text{mix}}^{\text{bcc}}(x)$ and $\Delta F_{\text{vibr}}(x)$ [see formula (5)]. Further improvement of the MCE fit, especially for fcc Fe-Cr, and the vibrational free-energy calculation as a function of alloy concentration, is necessary to improve the agreement between the calculated and experimentally observed shape of the γ -loop region in the T - x phase diagram.

IV. CONCLUSION

The MCE model reveals the microscopic physical origin of structural phase transitions in iron at high temperatures. The temperature variation of the two magnetic terms contributing to the free energy and shown in Fig. 2 exhibits opposing trends: the magnetic-energy difference decreases as a function of temperature whereas the magnetic-entropy term increases. When combined together, they result in a magnetic free-energy curve that has a minimum at a temperature above the Curie point. Adding the vibrational free-energy difference, which at these temperatures is an almost linear function of T , we arrive at a curve that intersects the temperature axis at two points, indicating the occurrence of α - γ and γ - δ structural phase transitions. Since the difference between the free energies of the two phases is very small, further improvement in the numerical accuracy of the calculations is necessary. For example, the model used in this work relies, in addition to the MCE-based Monte Carlo simulations for the magnetic part of the free energy, on experimental informa-

tion about the vibrational spectra of competing α and γ phases, which is only available for the nonoverlapping regions of the phase diagram where each individual phase is mechanically stable. There is a gap of approximately 250 K between the highest temperature at which experimental measurements of elastic constants for bcc Fe were performed and the only point for which experimental data are available for fcc Fe. Also, here we neglected the anharmonic contribution to the vibrational free energies of both structures. We realize that, given the small differences between the free energies of the competing phases, even small changes in the vibrational free energy could lead to either a large increase in the stability region for fcc Fe, or to the complete disappearance of this region. For example, by varying the elastic constants of either of the two phases by one percent we find that the vibrational free energy at $T=1500$ K changes by 2 meV/atom, which is greater than the predicted α - γ free-energy difference of 1.2 meV/atom. Future work is required to address this phase stability problem by treating the vibrational dynamics of Fe and Fe-Cr alloy on equal footing with configurational and magnetic properties of the system.

We conclude that the MCE model, which uses *ab initio*-derived magnetic interaction and symmetry-breaking parameters, and experimentally observed values of elastic moduli, is able to describe, at a quantitative level of accuracy, various magnetic and structural phase transitions occurring in Fe-Cr magnetic alloys. It appears possible, by relying only on the zero-temperature *ab initio* data, to evaluate parameters describing thermal magnetic fluctuations in the alloy.

The model correctly predicts the occurrence of two structural phase transitions occurring below the melting point and above the Curie temperature for pure Fe and for a range of Fe-Cr alloy compositions. An important advantage of the MCE model described in this paper is that it can be easily generalized to other magnetic alloys, including alloys of magnetic and nonmagnetic metals, such as Fe-Cr-V. The symmetry-breaking Hamiltonian (1) can readily treat ions with nonzero and zero magnetic moments by simply varying the sign of the on-site Landau coefficient A . This flexibility makes it possible to apply the MCE method to a broad range of alloy compositions involving magnetic and nonmagnetic atoms.

ACKNOWLEDGMENTS

We are grateful to J.-L. Boutard and D. G. Pettifor for stimulating discussions. This work was funded partly by the United Kingdom Engineering and Physical Sciences Research Council under Grant No. EP/G003955 and the European Communities under the contract of Association between EURATOM and CCFE.

- ¹S. L. Dudarev, J.-L. Boutard, R. Lässer, M. J. Caturla, P. M. Derlet, M. Fivel, C.-C. Fu, M. Y. Lavrentiev, L. Malerba, M. Mrovec, D. Nguyen-Manh, K. Nordlund, M. Perlado, R. Schäublin, H. Van Swygenhoven, D. Terentyev, J. Wallenius, D. Weygand, and F. Willaime, *J. Nucl. Mater.* **386-388**, 1 (2009).
- ²H. Hasegawa and D. G. Pettifor, *Phys. Rev. Lett.* **50**, 130 (1983).
- ³Yu. N. Osetsky and A. Serra, *Phys. Rev. B* **57**, 755 (1998).
- ⁴M. Müller, P. Erhart, and K. Albe, *J. Phys.: Condens. Matter* **19**, 326220 (2007).
- ⁵F. Körmann, A. Dick, B. Grabowski, B. Hallstedt, T. Hickel, and J. Neugebauer, *Phys. Rev. B* **78**, 033102 (2008).
- ⁶Q. Chen and B. Sundman, *J. Phase Equilibria* **22**, 631 (2001).
- ⁷R. J. Weiss and K. J. Tauer, *Phys. Rev.* **102**, 1490 (1956).
- ⁸W. Pepperhoff and M. Acet, *Constitution and Magnetism of Iron and Its Alloys* (Springer, Heidelberg, 2001).
- ⁹H. C. Herper, E. Hoffmann, and P. Entel, *Phys. Rev. B* **60**, 3839 (1999).
- ¹⁰E. Sjöstedt and L. Nordström, *Phys. Rev. B* **66**, 014447 (2002).
- ¹¹S. Shallcross, A. E. Kissavos, S. Sharma, and V. Meded, *Phys. Rev. B* **73**, 104443 (2006).
- ¹²Y. Tsunoda, *J. Phys.: Condens. Matter* **1**, 10427 (1989).
- ¹³A. Onodera, Y. Tsunoda, N. Kunitomi, O. A. Pringle, R. M. Nicklow, and R. M. Moon, *Phys. Rev. B* **50**, 3532 (1994).
- ¹⁴G. Y. Guo and H. H. Wang, *Phys. Rev. B* **62**, 5136 (2000).
- ¹⁵M. Černý, J. Pokluda, M. Šob, M. Friák, and P. Šandera, *Phys. Rev. B* **67**, 035116 (2003).
- ¹⁶P. Olsson, I. A. Abrikosov, L. Vitos, and J. Wallenius, *J. Nucl. Mater.* **321**, 84 (2003).
- ¹⁷A. A. Mirzoev, M. M. Yalalov, and D. A. Mirzaev, *Phys. Met. Metallogr.* **103**, 83 (2007).
- ¹⁸G. Kirchner, T. Nishizawa, and B. Uhrenius, *Metall. Trans.* **4**, 167 (1973).
- ¹⁹J. Chipman, *Metall. Trans.* **5**, 521 (1974).
- ²⁰M. Yu. Lavrentiev, S. L. Dudarev, and D. Nguyen-Manh, *J. Nucl. Mater.* **386-388**, 22 (2009).
- ²¹J. M. Sanchez, F. Ducastelle, and D. Gratias, *Physica A* **128**, 334 (1984).
- ²²M. Yu. Lavrentiev, R. Drautz, D. Nguyen-Manh, T. P. C. Klaver, and S. L. Dudarev, *Phys. Rev. B* **75**, 014208 (2007).
- ²³R. Drautz and M. Fähnle, *Phys. Rev. B* **69**, 104404 (2004); R. Singer and M. Fähnle, *J. Math. Phys.* **47**, 113503 (2006).
- ²⁴R. Drautz and M. Fähnle, *Phys. Rev. B* **72**, 212405 (2005).
- ²⁵G. J. Ackland, *Phys. Rev. Lett.* **97**, 015502 (2006); G. J. Ackland, *Phys. Rev. B* **79**, 094202 (2009).
- ²⁶S. L. Dudarev and P. M. Derlet, *J. Phys.: Condens. Matter* **17**, 7097 (2005); P. M. Derlet and S. L. Dudarev, *Prog. Mater. Sci.* **52**, 299 (2007).
- ²⁷D. Nguyen-Manh and S. L. Dudarev, *Phys. Rev. B* **80**, 104440 (2009).
- ²⁸G. Kresse and J. Hafner, *Phys. Rev. B* **49**, 14251 (1994); G. Kresse and J. Furthmüller, *ibid.* **54**, 11169 (1996); G. Kresse and D. Joubert, *ibid.* **59**, 1758 (1999).
- ²⁹D. J. Dever, *J. Appl. Phys.* **43**, 3293 (1972).
- ³⁰H. Hasegawa, M. W. Finnis, and D. G. Pettifor, *J. Phys. F: Met. Phys.* **17**, 2049 (1987).
- ³¹J. Zarestky and C. Stassis, *Phys. Rev. B* **35**, 4500 (1987).
- ³²X. Sha and R. E. Cohen, *Phys. Rev. B* **74**, 214111 (2006).
- ³³G. Bonny, R. C. Pasianot, L. Malerba, A. Caro, P. Olsson, and M. Yu. Lavrentiev, *J. Nucl. Mater.* **385**, 268 (2009).
- ³⁴D. Nguyen-Manh, M. Yu. Lavrentiev, and S. L. Dudarev, *C. R. Phys.* **9**, 379 (2008).
- ³⁵B. Fultz, L. Anthony, J. L. Robertson, R. M. Nicklow, S. Spooner, and M. Mostoller, *Phys. Rev. B* **52**, 3280 (1995).
- ³⁶A. Teklu, H. Ledbetter, S. Kim, L. A. Boatner, M. McGuire, and V. Keppens, *Metall. Mater. Trans. A* **35**, 3149 (2004).